Equilibration of granular subsystems†

F. Lechenault[a] and Karen E. Daniels*[b]

Received 21st December 2009, Accepted 25th February 2010
First published as an Advance Article on the web 14th April 2010
DOI: 10.1039/b926754a

We experimentally investigate the steady states of two granular assemblies differing in their material properties and allowed to exchange volume with each other under external agitation in the vicinity of their jamming transition. We extract the statistics of various static and dynamic quantities, and uncover a materials-independent relationship between the average packing fraction and its fluctuations. This relationship defines an intensive parameter which decouples from the volume statistics, and remarkably takes the same value in both subsystems. We also observe that an effective diffusion coefficient also takes the same value in each subsystem, even as the structural relaxation time increases over several orders of magnitude. These observations provide strong constraints on the eventual establishment of a granular equation of state.

1 Introduction

Statistical mechanics has proven to be one of the most powerful tools for understanding transitions between states in physical systems. This predictive power has been successfully extended to gently perturbed systems through linear response theory.[1] Such an approach emphasizes the significance of *intensive* state variables, analogous to temperature or pressure in equilibrium systems, but potentially extends their relevance to the wider spectrum of out-of-equilibrium systems. However, this formalism is not valid for systems driven far from equilibrium, even when in well defined steady states. It remains an open question whether or not state variables can be defined in a generic way for non-equilibrium steady states. The hope is that such state variables would carry predictive power regarding the system's response to a change in the driving parameters, or its behavior when put in contact with another system.

A key situation in which such tools are expected to be relevant is that of granular materials: systems composed of individual particles large enough to be insensitive to thermal fluctuations. Such materials are ubiquitous in natural and industrial contexts, and models of their dynamics would benefit from an improved understanding of how to prepare and manipulate them in well-defined macrostates determined by a small set of control parameters analogous to thermal intensivities. Promising measures of the temperature-like Edwards compactivity[2,3] have been made in static granular systems,[4–6] as well as Kubo-type fluctuation/response pairs[7] leading to effective temperature measurements in dynamic granular systems.[8–11] However, it remains an open question to what extent these temperature-like variables behave as true temperatures.

For granular materials under strong agitation, the interactions of individual particles are dominated by binary collisions. Such dynamics are well-described by a thermal-like kinetic theory in which the velocity fluctuations play the role of temperature.[12,13] However, the denser states relevant to many important granular flows are dominated by multi-body interactions and such states remain difficult to model through kinetic theory approaches.[14] The phenomenology of these dense states is strikingly reminiscent of supercooled liquids,[15–20] where classical statistical mechanics also loses validity due to a loss of ergodicity. Both the thermodynamic glass transition and the jamming transition in dense granular materials lack a fundamental understanding, and both have been hampered by the difficulty of making a relevant quantitative description of the state of the system. This universal phenomenology, embodied by a dramatic slowing down of the dynamics,[21] caging,[22–24] and memory effects,[25–28] is now referred to as the *jamming* transition, and is at the heart of a very active field of research which is the subject of this special issue.

Thermodynamics is founded on, among other things, a meaningful equilibration of intensive state variables between subsystems. Thus, if a thermodynamic-like description of granular materials is to be found, an informative first step would be to search for an analog of the zeroth law of thermodynamics. By putting two athermal systems in contact and allowing them to reach a steady state, one can seek relevant intensive parameters by discarding properties that fail to equilibrate. We experimentally conduct such an investigation, putting two model granular subsystems in contact.

In our experiments, we allow two adjacent monolayers of particles, differing in material properties, to exchange volume with each other under external agitation and an overall constant-volume constraint. We study the steady-state properties of the two subsystems as a function of the overall average packing fraction in the vicinity of their jamming transition. Importantly, we uncover a materials-independent relationship between the average packing fraction and its fluctuations. This relationship defines an intensive parameter that decouples from the volume statistics of the subsystems, and remarkably takes the same value in both subsystems. This observation provides a strong constraint on the eventual establishment of a granular equation of state. Moreover, among various dynamical quantities studied,

[a]*Department of Physics, NC State University, Raleigh, NC, USA*
[b]*Department of Physics, NC State University, Raleigh, NC, USA. E-mail: kdaniel@ncsu.edu*

† This paper is part of a *Soft Matter* themed issue on Granular and jammed materials. Guest editors: Andrea Liu and Sidney Nagel.

an effective diffusion coefficient is shown to take the same value in the "equilibrated" subsystems, while the structural relaxation times exhibit different behaviors. While a thermodynamic system would lead to temperature equilibration, the present situation leads to a decoupling of the mobility and the structural relaxation time, and only the former seems to yield relevant information about the properties shared by subsystems in steady states. Remarkably, this decoupling of the dynamics occurs in the vicinity of the *static* random loose packing.

2 Experimental setup and protocol

We study the equilibration of two adjacent dense bidisperse layers of disks on an air table, as sketched in Fig. 1. A piston separates the two subsystems, and is constrained to move along the long axis of the air table by protruding feet which impede rotation. On each side of the table, the system is prepared with an identical number of particles N, with the ratio of small to large particles fixed at $N_S = 2N_L$. This ratio suppresses crystallization and provides roughly the same volume of large (diameter $d_L = 86$ mm) and small particles ($d_S = 58$ mm). The particles within each subsystem have a different set of material properties: on Side 1, the particles have restitution coefficient $\varepsilon_1 = 0.51 \pm 0.07$ and friction coefficient $\mu_1 = 0.85$; on Side 2, the particles have $\varepsilon_2 = 0.33 \pm 0.03$ and $\mu_2 = 0.5$. Restitution coefficients were measured from isolated binary collisions; friction coefficients are nominal values from the literature. Both sides utilize standard plastic Petri dishes as the particles, with the difference in particle properties achieved by encircling the particles on Side 1 with a rubber band. Because the sides of the particles slope inwards, the thickness of the rubber band does not significantly change the radius of the particles; the mass of the particles on Side 1 is increased by 7%.

The aggregate rearranges *via* an array of sixty electromagnetic bumpers which form the walls of the system. These bumpers are triggered pairwise: bumpers facing each other in the system fire at the same time in order to prevent net momentum and torque injection. These pairs are triggered randomly *via* a pre-generated random sequence. Four pairs of bumpers are randomly fired every 0.1 s, and travel 1 cm into the granular pack; the total time during which the bumpers stay in their forward position is approximately 0.1 s.

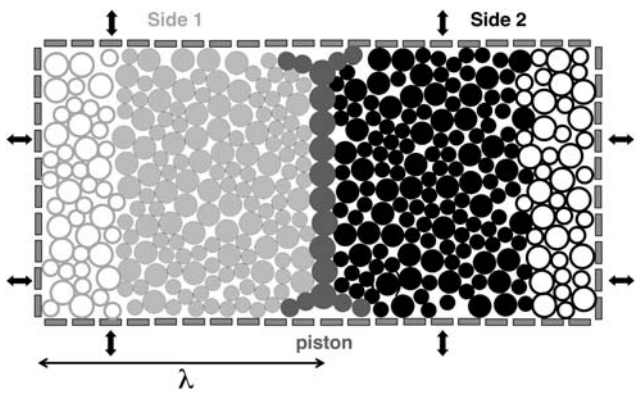

Fig. 1 Apparatus schematic (1 m × 2 m), with particles drawn to scale. Filled particles are taken from an experimental configuration and indicate the size of the imaged region. λ between 0 and 1 measures the fractional position of the piston.

To quantify the long-time mobility of the particles, we take images at a frequency which is low compared to the energy injection timescale, making usual tracking techniques inoperative. Therefore, we have developed a tracking method which identifies each particle by a unique tag. Each particle is marked with a 3 × 3 array of colored dots which encodes two copies of a 4-bit, 4-digit identifier, plus an error-correcting bit. The particles are located by their circular rims and their identities are established using the tags, allowing their positions in adjacent image frames to be connected into trajectories. We monitor the positions of the piston and the inner 75% of the particles with a CCD camera mounted above the apparatus; we obtain a minimum of 10^4 configurations for each experiment.

To understand the equilibration of the system on its approach to jamming, we perform experiments at increasing values of N while holding all other variables constant. We adjust N in increments of 2 small and 1 large particle on each side, so that the two sides always have the same N. The average packing fraction $\bar{\phi}$ calculated for the entire system is given by

$$\bar{\phi} \equiv 2\left(\frac{1}{\langle\phi_1\rangle} + \frac{1}{\langle\phi_2\rangle}\right)^{-1} \quad (1)$$

as well as by the ratio of the total area of N disks to the total area of the air table. As we adjust N from 183 to 204, this corresponds to $\bar{\phi} = 0.768$ to 0.818.

3 Macroscopic observables

First we focus on the macroscopic state of the system, namely the volume occupied by each of the subsystems. Since the overall volume of the system is conserved, we only need to consider the position of the piston scaled by the length of the cell $0 < \lambda < 1$, where the origin of the axis is taken on the side occupied by the particles that have been circled by a rubber band, referred to as Side 1 in the following discussion.

We first consider the time signal $\lambda(t)$ for a given value of N, an example of which is displayed in Fig. 2a. After a transient time τ_R, the signal becomes stationary and the system has reached a steady state. This state is observed for all reported values of N. Note that τ_R is comparable to, though smaller than, the α-relaxation time τ_α of the assembly, *i.e.* the time it takes for the particles to diffuse further that their size.[29] We thus conservatively discard data for $\tau < \tau_\alpha$ and consider the probability distribution of λ in this stationary regime and we find Gaussian statistics even for the largest N (densest $\bar{\phi}$); sample distributions are shown in Fig. 2b.

These statistics are thus characterized by the first two moments. We observe that the average piston position $\langle\lambda\rangle \equiv \langle\lambda(t)\rangle_t$ is observed to be $\leq$½ for all values of N: Side 1, containing the particles with rubber bands, occupies less volume than the side without. The error on $\langle\lambda\rangle$ is $\pm$ 0.001, estimated from both control runs with identical particles and repeated runs at the same parameter values, visible as the gray points in Fig. 3. We conclude that this systematic deviation from equal volumes originates from the difference in material properties of the particles. Furthermore, and rather surprisingly, $\langle\lambda\rangle$ is not a monotonic function of N: it increases until it reaches ½ for

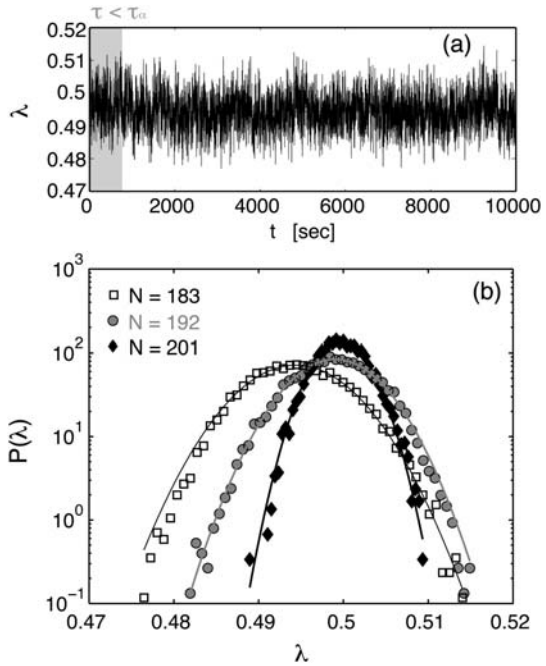

Fig. 2 (a) Scaled piston position $\lambda(t)$ for $N = 201$ ($\bar{\phi} = 0.812$). (b) Sample probability density functions of λ (and Gaussian fits) for $N = 183$, 192 and 201 ($\bar{\phi} = 0.766$, 0.789, 0.812).

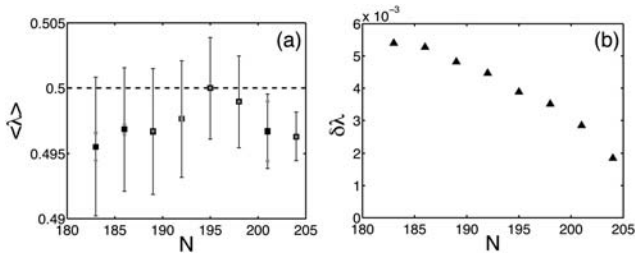

Fig. 3 (a) $\langle\lambda\rangle$ (Side 1) as a function of N, with bars representing the standard deviation. For some values of N, the experiment has been repeated several times starting from different initial configurations, in order to evaluate the errors; these measurements are shown as smaller symbols. (b) Standard deviation $\delta\lambda$ as a function of N.

$N^* = 195$ and then decreases for larger values of N. At this crossover, the packing fraction is equal on both sides, $\phi^* = 0.798$. The behavior of the system is qualitatively different on each side of this transition point. For values of $N \leq N^*$, the particles interact mostly through short binary collisions and the system looks liquid-like. For $N \geq N^*$, the dynamics are dominated by multi-body interactions and become much slower. In watching the system, intermittent force chains[30] are observed to carry the motion imposed by the boundaries into the bulk of the system, and some particles stay in contact with one another on time scales larger than the typical collision time. However, no permanent stress seems to be trapped in the system until it jams: this occurs at the highest explored value of N as will be quantified below.

Interestingly, this transition at $\phi^* = 0.798$ is close to, but perhaps slightly below, independent measurements of random loose packing for these particles: $\phi^{RLP}{}_1 = 0.807 \pm 0.010$ and $\phi^{RLP}{}_2 = 0.812 \pm 0.006$. To determine ϕ^{RLP} for each of the two types of particles, we placed the table at a 0.3° angle, and rained down single particles from the high end to the low end to create the loosest packing accessible to us. These values are upper bounds for random loose packing, for our protocol does not guarantee that we reach the loosest possible stable packs.

The standard deviation of these distributions, $\delta\lambda \equiv \sqrt{\langle\lambda^2\rangle - \langle\lambda\rangle^2}$, exhibits a simpler behavior: it is a decreasing function of N, as can be seen in Fig. 3b. This is to be expected from the fact that as N increases a smaller amount of free volume is available for the motion of the piston. Notably, this quantity does not exhibit any special feature in the vicinity of N^*. Finally, the magnitude of $\delta\lambda$ at the highest explored value of N closely matches the volume fluctuations imposed by the bumpers. This mean that this macroscopic quantity becomes trivial when the system approaches its jammed state, merely reproducing the microscopic fluctuations imposed by the injection mechanism. However, even in the densest state explored the system is not strictly rigid: particles continue to rearrange due to the impacts from the boundaries.

4 Microscopic observables

4.1 Statics

We now turn to the microscopic information provided by particle-tracking. In order to extract a well-defined, size-independent microscopic quantity from the packing fraction field, we analyze the spatial and temporal fluctuations of the average local

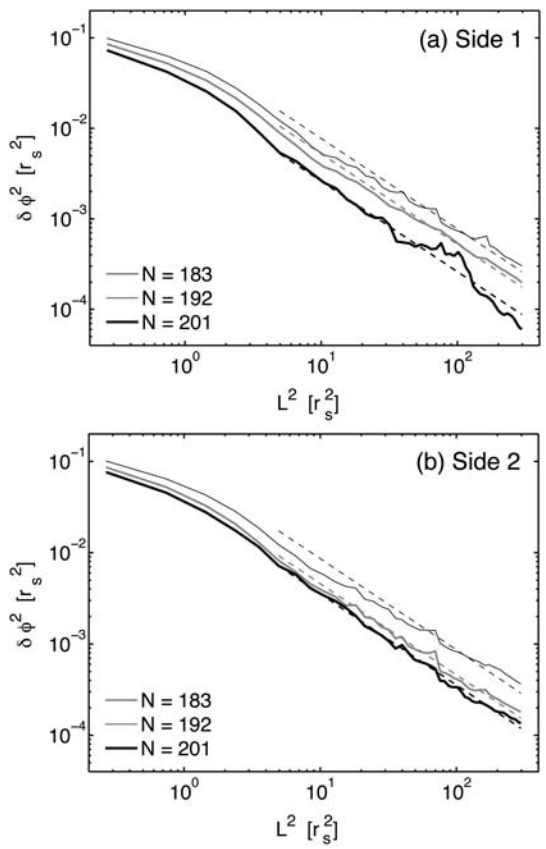

Fig. 4 Variance $\langle\delta\phi^2\rangle$ of the packing fraction measured within squares of size L for three values of N; dashed lines are $\langle\delta\phi^2\rangle_0/L^2$.

packing fraction ϕ over windows of increasing size, where ϕ is defined as the ratio of the number of pixels occupied by the particles to the total number of pixels in a given region. For each subsystem, we measure ϕ over boxes of size L ranging from a few $r_s = \frac{1}{2}d_s$ up to half the system size. For $L \gtrsim 2r_s$, $\phi(L)$ converges to a constant. Moreover, the variance $\langle \delta\phi^2 \rangle$ scales approximately as L^{-2}, as shown in Fig. 4. Such scaling behavior is expected from the central limit theorem provided there are no long-ranged spatial correlations in the packing fraction field. Since the packing fraction does not exhibit such correlations, it is suitable for a thermodynamic-like analysis despite the relatively small number of particles. Furthermore, we obtain an L-independent measure of the variance of ϕ by averaging $\langle \delta\phi^2 \rangle_0 \equiv \langle \delta\phi^2 \rangle L^2$ over all $L > 2r_S$.

These two packing fraction statistics are plotted as a function of N in Fig. 5: $\langle \phi \rangle$ is higher for Side 1, in agreement with our macroscopic measurement. Similarly, at $N = 195$ the packing fractions are equal ($\langle \phi \rangle = \bar{\phi} = 0.798$ for both sides). Different values of the normalized ϕ fluctuations $\langle \delta\phi^2 \rangle_0$ are observed on the two equilibrated sides, indicating that the statistics of this quantity depend on the material properties. Moreover, the fluctuations on each side are found to be decreasing functions of N, as shown in Fig. 5b. As for the fluctuations of λ, these can be understood by the fact that as N increases, the amount of free volume to be distributed among the particles decreases. Finally, the discrepancy in the packing fraction statistics between the two sides gets larger on approach to jamming at large $\bar{\phi}$ (large N), especially as the number of particles is increased above N^*.

To examine the relevance of these two state variables, we plot the dependence of $\langle \delta\phi^2 \rangle_0$ on $\langle \phi \rangle$, parametrized by N (see Fig. 5c). Remarkably, the data from both sides fall onto a single master curve: the fluctuations in local ϕ are *insensitive* to the material properties of the particles. Within the explored range of N, this master curve is approximately linear and the extrapolation would intersect $\langle \delta\phi^2 \rangle_0 = 0$ at $\langle \phi \rangle = \phi_J = 0.848 \pm 0.003$ which is compatible with the rigidity transition reported in other bidimensional systems.[20,31,32] This result therefore stands as a starting point for a granular equation of state. It is notable that, as in Fig. 5b, the transition at $N^* = 195$ does not appear as a feature.

4.2 Dynamics

We now turn to the microscopic characterization of the dynamics in our system as the system transitions from a liquid-like to a solid-like state. To monitor this transition, we use particle-trajectories to compute the average diffusion distance as a function of lag-time τ, defined as

$$\sigma(\tau) \equiv \sqrt{\left\langle \| \vec{r}_i(t+\tau) - \vec{r}_i(t) \|^2 \right\rangle_{i,t}} \qquad (2)$$

where $\vec{r}_i(t)$ is the vector position of particle i at time t. Averages are computed over the ensemble of all particle trajectories at all times.

Fig. 6 shows how the r.m.s. displacement $\sigma(\tau)$ and the corresponding particle trajectories vary as increasing N brings the system towards jamming. At $N = 183$ (low $\bar{\phi}$) a particle explores

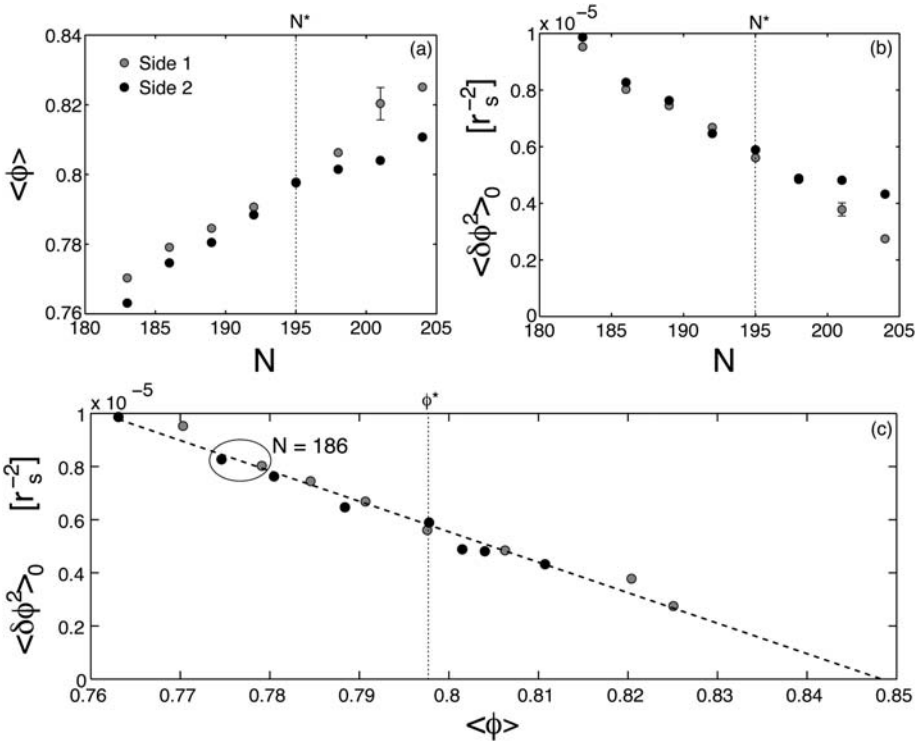

Fig. 5 (a) Packing fraction $\langle \phi \rangle$ and (b) normalized packing fraction fluctuations $\langle \delta\phi^2 \rangle_0$ as a function of number of particles on each side. (c) Data from parts (a) and (b) combined on a single plot without regard for N. Ellipse encloses two points obtained from Side 1 (grey) and Side 2 (black) for a single run with $N = 186$. Dashed line is a linear fit to data from both sides, showing an intercept at $\phi_J = 0.848$. For comparison, $N^* = 195$ corresponds to $\phi^* = 0.798$.

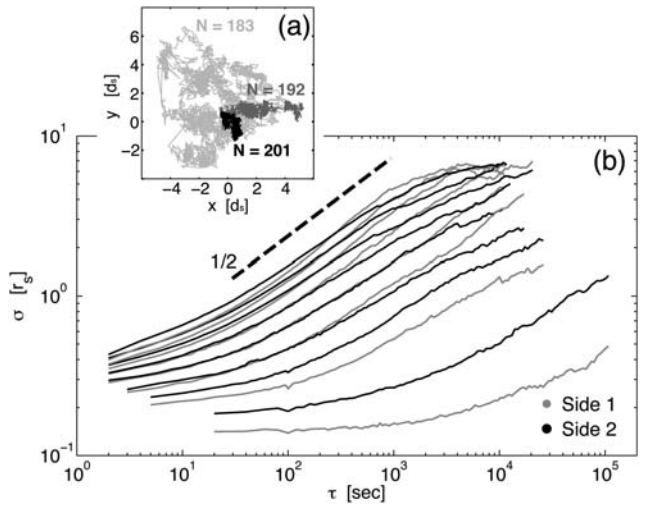

Fig. 6 (a) Trajectories of a single particle (from Side 1) for a duration of 10^4 s. (b) Diffusion length σ as a function of lag-time τ. Grey lines are for Side 1; black lines are for Side 2. Dashed line is $\sigma \propto \tau^{1/2}$ to guide the eye.

a region several r_s wide, and σ saturates at long time scales due to finite system size. On the other hand, at $N = 201$ (high $\bar{\phi}$), σ exhibits sub-diffusive behavior at short τ, and caging effects are significant. As the dynamics of the system slow down at large N, we increase the duration of the experiment from twenty hours up to fifty-five hours for the densest packing in order to sample a significant set of configurations. However, even at this extended acquisition time, the diffusion length at $N = 201$ barely passes $1r_s$. Hence, beyond this point, the structure no longer rearranges over the experimental time and the system is in a glassy state.

In order to extract meaningful information from $\sigma(\tau)$, including establishing whether a truly diffusive regime is ever reached, we compute the local slope

$$\nu \equiv \frac{\partial(\log \sigma)}{\partial(\log \tau)}. \tag{3}$$

over a range of τ that allows for a reasonable estimation of the local slope. Interestingly, for all studied values of N this local exponent exhibits a maximum, as illustrated in Fig. 7. This maximum is consistently close to ½, as can be seen in Fig. 8b. However, the exponent ν is larger for Side 1 (rubber bands) than Side 2 (bare) for $N < N^*$. Side 1 changes from super-diffusive ($\nu > ½$) below N^* to sub-diffusive ($\nu < ½$) behavior above N^*. In contrast, Side 2 is sub-diffusive for all values of N.

We have extracted the characteristic time and length scales τ_M and σ_M at which this maximum is reached, plotted in Fig. 8. For both sides of the system, the time scale at which maximally-diffusive behavior is reached rises by two orders of magnitude as N approaches the jammed state, and the length scale falls. These quantities indicate the occurrence of a dynamical crossover at N^* since σ_M, τ_M, and ν all display different behavior above and below this value. Side 1 is more mobile for $N < N^*$ and Side 2 is more mobile above. Interestingly, this transition occurs when σ_M is close to the mean diameter of the grains ($\sigma_M = 2r_s$). This suggests that the local rearrangement mechanism governing the dynamics at the particle scale changes near N^*.

We use the behavior near (σ_M, τ_M) to extract quantities which quantify the diffusive behavior of the system. The structural relaxation time τ_α is obtained from the time at which $\sigma(\tau_\alpha)$ crosses r_s, meaning that the particles have diffused beyond their radius. A diffusion coefficient D is estimated by solving

$$\sigma_M = D\,\tau_M^{\frac{1}{2}} \tag{4}$$

for D. Since the dynamics of the system are not properly diffusive, this diffusion coefficient should be interpreted merely as a measure of the displacement amplitude at the time of maximum mobility. Astonishingly, as can be seen in Fig. 8, this definition for D provides a dynamical parameter that takes approximately the *same* value in each subsystem regardless of N.

Both D and τ_α indicate a slowing down for increasing N, as shown in Fig. 8. On both sides, D decreases monotonically to nearly zero for our last data point, indicative of the system's cessation of rearrangement (jamming). Meanwhile, as is usually observed in the vicinity of the glass/jamming transition, the structural relaxation time for both species of particles soars over multiple orders of magnitude. The plot of $\tau_\alpha(N)$ shows that both above and below N^*, Side 1 (rubber band particles) exhibits longer relaxation times than Side 2. As for ν, σ_M, and τ_M, the N^* crossover point is special in that these quantities each take the same value on both sides. No dramatic changes take place for $D(N)$ near N^*: it is remarkably equal in each subsystem for all values of N.

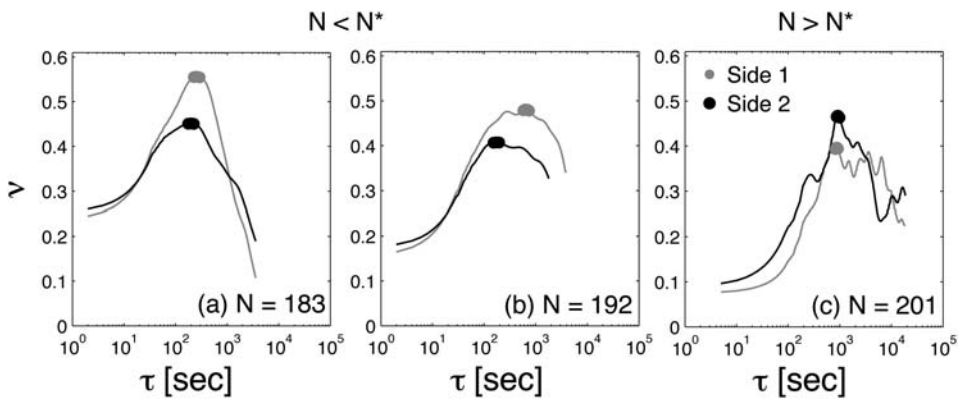

Fig. 7 Local exponent ν as a function of lag-time τ for $N = 183$, 192 and 201 for side 1 (grey) and side 2 (black). The thick region indicates the averaged maximum used to obtain a diffusion constant D from eqn (3).

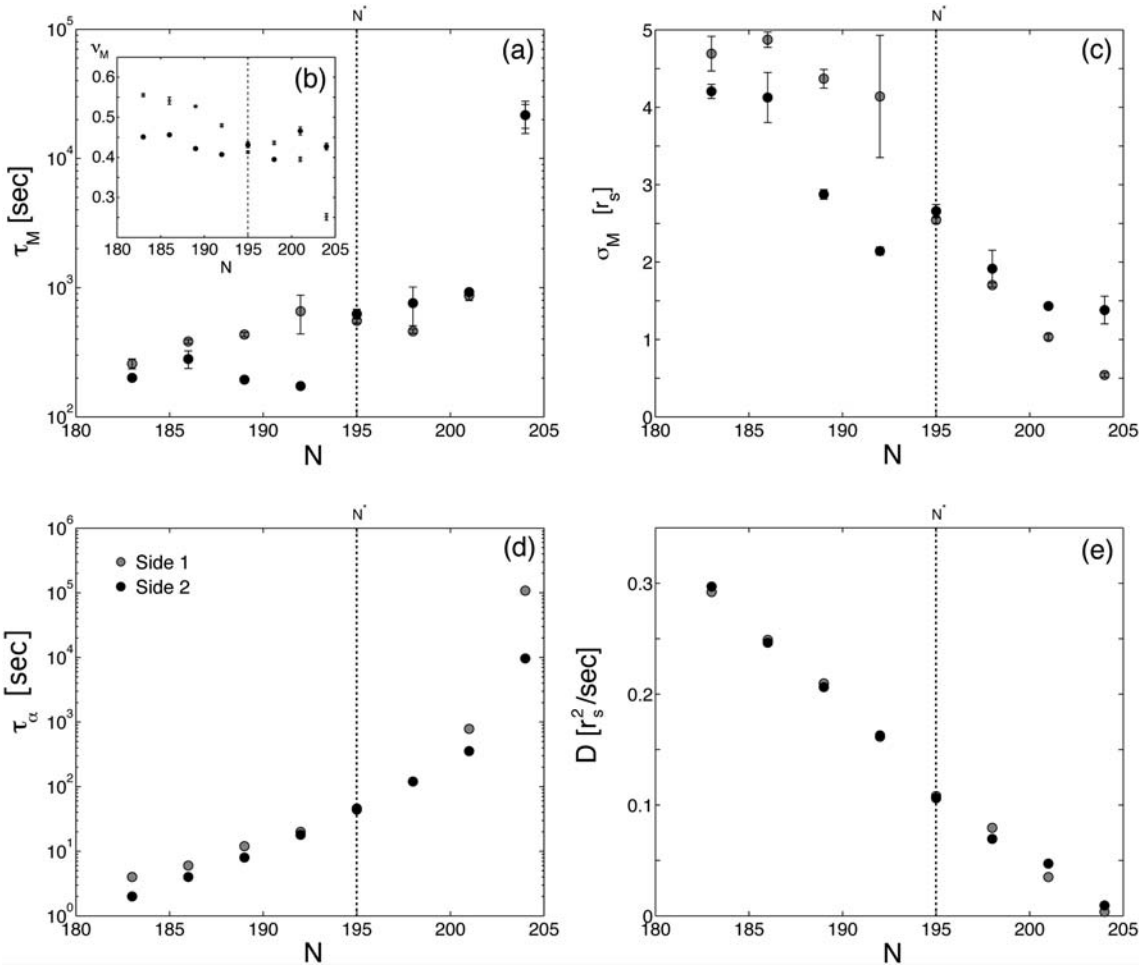

Fig. 8 Time scale τ_M at which the maximum exponent ν_M is reached (a) as a function of N for the two grain species (grey for side 1 and black for side 2). Corresponding values of ν_M (b inset) and σ_M (c). structural relaxation time τ_α (d) and diffusion coefficient D (e) as a function of N.

Since the timescale τ_α is observed to be sensitive to N^*, we investigate the extent to which the packing fraction is relevant to the dynamics. Therefore, we plot both D and τ_α as a function of $\langle\phi\rangle$ in Fig. 9. As in Fig. 5, pairs of data points from the same run are plotted at their corresponding values of $\langle\phi\rangle$. This parametrization predicts that $D(\phi)$ vanishes at different values for the two different particle types, with $\phi J^{(1)} > \phi J^{(2)}$. In examining $\tau_\alpha(\phi)$ for the two sides, there is a common (material-independent) branch of the curve for $\langle\phi\rangle \lesssim \phi^*$ which increases gradually. The value of $\langle\phi\rangle$ at which τ_α leaves this branch differs for the two types of particles, with Side 1 again having its transition at lower $\langle\phi\rangle$. This transition is associated with local rearrangement mechanisms, and likely corresponds to the packing fraction at which single-particle rearrangements are no longer possible.[33]

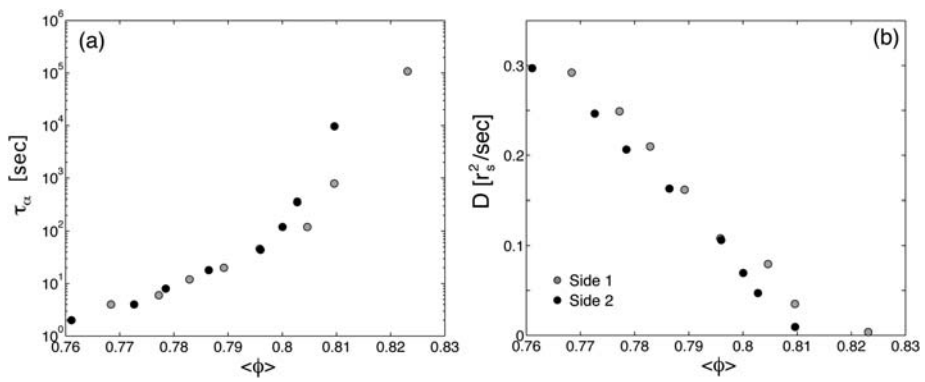

Fig. 9 (a) Structural relaxation time τ_α and (b) diffusion coefficient D as a function of $\langle\phi\rangle$ (without regard for N).

5 Discussion and conclusions

We have explored the stationary states of subsystems able to exchange volume, following them from a liquid-like to a jammed state. In order to examine the extent to which state variables and the density of states are useful tools to understand this transition, we would need to understand the role of energy, entropy, and our ability to identify the corresponding microstates. An analysis based on the generation of entropy through the braiding of trajectories[34,35] establishes the chaotic nature of the internal dynamics in our system. This, together with the stationarity, ensures the existence of an invariant measure, namely the Sinai–Ruelle–Bowen measure,[36] from which our temporal averages are guaranteed to correspond to ensemble averages. This provides a strong basis for the statistical analysis provided above and lends a thermodynamic-like status to the quantities extracted from our equilibration experiments. Within such a framework, our results suggest further interpretation.

In Fig. 5, we have uncovered an unexpected one-to-one relationship between the average local packing fraction $\langle\phi\rangle$ and its fluctuations $\langle\delta\phi^2\rangle_0$. This striking relationship, in which both N and the material properties collapse on a single curve, should be a prediction from an as-yet unknown equation of state. Interestingly, the function does not appear to be sensitive to the transition at $\phi^* \approx \phi^{RLP}$ which is a prominent feature in the equilibration measurements of the piston position (see Fig. 2).

To make use of the relationship, it is tempting to define a variable

$$Q \equiv \frac{\langle\delta\phi^2\rangle_0}{\langle\phi\rangle - \phi_J} \tag{5}$$

which is intensive, ϕ-independent, and takes the same value in both subsystems for all N. However, the value of Q, which we conjecture to be related to the energy injection and/or dissipation rates in the system, is not sufficient to specify the equilibrated volumes. This suggests that another parameter is needed to fully characterize the state of a dynamically evolving dense granular pack, much as both temperature and pressure equilibration are needed to solve the equivalent problem within classical thermodynamics. The present experiment does not allow us to measure the instantaneous kinetic and potential energies, but future studies of particle kinetics would allow further investigation of such parameters.

Diffusion measurements provide an alternative framework in which to understand the behavior of our system and hence the equilibration process. We have observed that the piston position λ, relaxation time τ_α, and the maximum mobility length and timescales (σ_M, τ_M) are sensitive to the transition at ϕ^* (see Fig. 2) which is close to the static ϕ^{RLP}. These changes in the dynamics suggest that the transition corresponds to two qualitatively different dynamical regimes. For $\phi < \phi^*$, the particles primarily interact through short binary collisions and there is weak coupling between the particles. Because the system is collision-dominated, it is likely that the restitution coefficients of the particles are an important consideration in the dynamics. If so, it would explain the observation that for Side 1 (larger coefficient of restitution), λ increases with N. For $\phi > \phi^*$, long multibody interactions dominate the dynamics, and we visually observe signs of intermittent force chains[30] which strongly couple both particle–particle and particle–bumper interactions. It is likely that the higher friction coefficient on Side 1 significantly increases the structural relaxation time of the corresponding assembly, and the dynamics are more sensitive to the frictional properties of the particles. Interestingly, all measured quantities are approximately equal in each subsystem at N^*.

As the system approaches ϕ_J, the persistence time of the contact network increases, and the internal response of the particles is more correlated. For the largest studied value of N, the packing fraction and overall volume fluctuations are imposed by the boundaries. Hardly any rearrangement occurs on experimentally-accessible time scales, but extended internal vibrations can be observed: the behavior of the system is thus comparable to that of a solid.

From a thermodynamic point of view, it is remarkable that the effective diffusion coefficients defined above are the only measured quantities to take the same value in the equilibrated subsystems, whereas the relaxation times τ_α become very different from each other beyond N^*. As a matter of fact, in equilibrium systems, the Stokes–Einstein relation states that the product of the diffusion coefficient and the viscosity (or, equivalently, the relaxation time), is proportional to temperature.[1] Hence, only the product $D\tau_\alpha$, and not D itself, is expected to equilibrate. Here, we find that there is a decoupling between the relaxation time and the diffusion coefficient beyond N^*, which is reminiscent of the decoupling reported in the vicinity of the glass transition in supercooled liquids,[37,38] the latter equilibrating while the former emphasizes the difference in material properties between the two sides. This phenomenon is yet another common feature between dense granular materials and supercooled liquids, and seems to indicate that fluctuation/response based temperatures might be relevant below ϕ^{RLP}.[15]

Thus, we observe that both packing fraction (or free volume) and material properties play a key role in determining the state of the system. In static granular systems, the Edwards ensemble[2] provides a framework for understanding how volume plays a central role in describing the density of states and associated Boltzmann-like thermodynamic properties. While our system is dynamic, it is interesting to ask to what extent the equilibration of volume between two subsystems exhibits features reminiscent of the Edwards formalism. The overall volume of our system is a conserved quantity, the dynamics explore a set of configurations (although not strictly mechanically-stable), and we achieve stationary distributions of system properties such as $\langle\phi\rangle$. Were volume the dominant state variable setting the density of states for this system, we would have observed $\lambda = ½$, independent of N. Instead, the material properties of the particles play an important role in dynamically determining the state of the system, and we observe that in general $\lambda \neq ½$.

In this paper, we have experimentally studied the steady state statistics of two model granular subsystems differing in their material properties put in contact through a mobile wall. We have uncovered several features that constrain any specification of a granular equation of state. First, most static and dynamical quantities are affected by a dynamical crossover which occurs at a packing fraction close to the (static) random loose packing. We interpret this crossover as separating the weak and strong coupling regimes in the behavior of the system. However, both the macroscopic volume fluctuations and the diffusion

coefficients are insensitive to this transition. Second, we have found that the packing fraction fluctuations are in a one-to-one correspondence with the average packing fraction, independent of the material properties of the grains. These fluctuations drop to zero on the approach to jamming. Finally, the diffusion properties of the particles reveal a glassy feature known as decoupling which arises above random loose packing. However, in spite of the fact that the structural relaxation timescale becomes both large and material-dependent for dense systems, the effective diffusion coefficient nonetheless takes the same value in each subsystem. This suggests that this coefficient is an important intensive parameter describing the state of the system. A theoretical understanding of these last two findings could come from the shrinking density of states on the approach to jamming. It is intriguing that the packing fraction fluctuations (geometry) suggest material-independence while the relaxation timescales (dynamics) suggest material-dependence.

References

1 R. Kubo, *Rep. Prog. Phys.*, 1966, **29**, 255–284.
2 S. F. Edwards and R. B. S. Oakeshott, *Phys. A*, 1989, **157**, 1080–1090.
3 A. Coniglio, A. Fierro, M. Nicodemi, M. P. Ciamarra and M. Tarzia, *J. Phys.: Condens. Matter*, 2005, **17**, S2557–S2572.
4 E. R. Nowak, J. B. Knight, E. Ben-Naim, H. M. Jaeger and S. R. Nagel, *Phys. Rev. E*, 1998, **57**, 1971–1982.
5 M. Schröter, D. I. Goldman and H. L. Swinney, *Phys. Rev. E*, 2005, **71**, 030301.
6 S. McNamara, P. Richard, S. de Richter, G. Le Caer and R. Delannay, *Phys. Rev. E*, 2009, **80**, 31301.
7 L. F. Cugliandolo, J. Kurchan and L. Peliti, *Phys. Rev. E*, 1997, **55**, 3898–3914.
8 G. D'Anna and G. Gremaud, *Nature*, 2001, **413**, 407–409.
9 N. Xu and C. S. O'Hern, *Phys. Rev. Lett.*, 2005, **94**, 055701.
10 F. Q. Potiguar and H. A. Makse, *Eur. Phys. J. E*, 2006, **19**, 171–183.
11 P. Wang, C. Song, C. Briscoe and H. A. Makse, *Phys. Rev. E*, 2008, **77**, 061309.
12 J. T. Jenkins and S. B. Savage, *J. Fluid Mech.*, 1983, **130**, 187–202.
13 C. K. K. Lun, S. B. Savage, D. J. Jeffrey and N. Chepurniy, *J. Fluid Mech.*, 1984, **140**, 223–256.
14 S. Moon, M. Shattuck and J. Swift, *Phys. Rev. E*, 2001, **64**, 31303.
15 A. J. Liu and S. R. Nagel, *Nature*, 1998, **396**, 21–22.
16 S. C. Glotzer, V. N. Novikov and T. B. Schrøder, *J. Chem. Phys.*, 2000, **112**, 509–512.
17 L. E. Silbert, *Phys. Rev. Lett.*, 2005, **94**, 098002.
18 A. R. Abate and D. J. Durian, *Phys. Rev. E*, 2006, **74**, 031308.
19 A. S. Keys, A. R. Abate, S. C. Glotzer and D. J. Durian, *Nat. Phys.*, 2007, **3**, 260–264.
20 F. Lechenault, O. Dauchot, G. Biroli and J. P. Bouchaud, *Europhys. Lett.*, 2008, **83**, 46003.
21 P. Mayor, G. D'Anna and G. Gremaud, *Mater. Sci. Eng., A*, 2004, **370**, 307–310.
22 E. R. Weeks and D. A. Weitz, *Phys. Rev. Lett.*, 2002, **89**, 095704.
23 O. Dauchot, G. Marty and G. Biroli, *Phys. Rev. Lett.*, 2005, **95**, 265701.
24 P. M. Reis, R. A. Ingale and M. D. Shattuck, *Phys. Rev. Lett.*, 2007, **98**, 188301.
25 C. Josserand, A. V. Tkachenko, D. M. Mueth and H. M. Jaeger, *Phys. Rev. Lett.*, 2000, **85**, 3632–3635.
26 L. Berthier and J. P. Bouchaud, *Phys. Rev. B*, 2002, **66**, 054404.
27 L. Berthier and P. C. W. Holdsworth, *Europhys. Lett.*, 2002, **58**, 35–41.
28 S. J. Friedmann, G. Kwon and W. Losert, *J. Geophys. Res.*, 2003, **108**, 2380.
29 G. Lois, J. Blawzdziewicz and C. S. O'Hern, *Phys. Rev. Lett.*, 2009, **102**, 015702.
30 A. Ferguson and B. Chakraborty, *Europhys. Lett.*, 2007, **78**, 28003.
31 C. S. O'Hern, L. E. Silbert, A. J. Liu and S. R. Nagel, *Phys. Rev. E*, 2003, **68**, 011306.
32 T. S. Majmudar, M. Sperl, S. Luding and R. P. Behringer, *Phys. Rev. Lett.*, 2007, **98**, 058001.
33 T. Aste, *J. Phys.: Condens. Matter*, 2005, **17**, S2361–S2390.
34 J. L. Thiffeault, *Phys. Rev. Lett.*, 2005, **94**, 084502.
35 J. G. Puckett, F. Lechenault and K. E. Daniels, *Powders and Grains 2009: Proceedings of the 6th International Conference on Micromechanics of Granular Media*, 2009, pp. 675–678.
36 J.-P. Eckmann and D. Ruelle, *Rev. Mod. Phys.*, 1985, **57**, 617–656.
37 F. Fujara, B. Geil, H. Sillescu and G. Fleischer, *Zeitschrift fur Physik B Condensed Matter*, 1992, **88**, 195–204.
38 P. Debenedetti and F. Stillinger, *Nature*, 2001, **410**, 259–267.